machines

MDPI

Article

Fuzzy-PID-Enhanced Fractional-Order Terminal Sliding Mode Control for Robotic Manipulator Trajectory Tracking Under Uncertainties

Jian Liu, Shicai Shi *, Zhiqi Li, Minghe Jin and Hong Liu

State Key Laboratory of Robotics and System, Harbin Institute of Technology, Harbin 150001, China
* Correspondence: sschit@hit.edu.cn

Abstract

Accurate and rapid trajectory tracking of robotic manipulators remains challenging due to model uncertainties, friction effects, and unknown external disturbances. Although fractional-order sliding mode control and disturbance observers have been widely investigated, achieving fast convergence, high tracking accuracy, and effective disturbance compensation within a unified control framework remains challenging. To address these issues, this paper proposes a Fuzzy-PID–Enhanced Fractional-Order Terminal Sliding Mode Control (Fuzzy PID-FOTSMC) integrated with an Improved Fractional-Order Disturbance Observer (IFODOB). The IFODOB estimates lumped uncertainties and external disturbances to provide feedforward compensation, while a fractional-order PID-type terminal sliding surface is constructed to improve tracking performance. Furthermore, a fuzzy logic mechanism is introduced to adaptively adjust the PID gains according to tracking errors. Lyapunov-based analysis is conducted to establish the stability and finite-time convergence properties of the proposed observer and controller under the stated assumptions. Numerical simulations are performed using a planar two-degree-of-freedom robotic manipulator under model uncertainties, friction, and external disturbances. Compared with the conventional FODOB, the proposed IFODOB reduces the disturbance-estimation convergence time from 1.20 s to 0.26 s for Joint 1 and from 1.30 s to 0.27 s for Joint 2. Furthermore, the proposed controller achieves position-tracking convergence times of 0.223 s and 0.556 s for the two joints, respectively, outperforming the three benchmark controllers in terms of convergence speed and steady-state tracking accuracy. These results demonstrate the effectiveness of the proposed observer–controller framework for robust and high-precision robotic manipulator trajectory tracking.

Keywords: trajectory tracking; uncertainties; fractional-order; fuzzy mechanism; sliding mode control; disturbance observer

Check for updates

Academic Editor: Carmine Maria Pappalardo

Received: 18 October 2026
Revised: 13 November 2026
Accepted: 16 November 2026
Published: 18 November 2026

Copyright: © 2026 by the authors. Licensee MDPI, Basel, Switzerland. This article is an open access article distributed under the terms and conditions of the Creative Commons Attribution (CC BY) license.

1. Introduction

Robotic manipulators are important for space servicing tasks, including satellite repair, refueling, debris removal, and structural assembly [1–3], and have potential applications in underwater exploration and subsea operations [4]. These applications require reliable trajectory tracking despite uncertain inertial parameters, joint friction, external disturbances, and payload variations [5–7]. Such complexities motivate robust control strategies that can maintain tracking performance in uncertain operating conditions. Furthermore, robust manipulator control may contribute to the United Nations Sustainable Development Goals

(UN-SDGs), particularly SDG 9 (Industry, Innovation and Infrastructure) through precision automation and SDG 14 (Life Below Water) through underwater robotic applications [8].

A variety of control strategies have been developed for nonlinear robotic systems, including proportional–integral–derivative (PID) control [9], model predictive control [10], sliding mode control (SMC) [11], adaptive control [12], and robust control [13]. SMC is attractive because of its robustness to matched uncertainties, and its application to robot tracking has a long history [14]. However, conventional linear sliding surfaces may exhibit chattering and generally provide asymptotic rather than finite-time convergence. Terminal sliding mode control and its nonsingular or fast variants have therefore been investigated to accelerate convergence [15–19]. Integral sliding and dynamic-surface approaches have also been explored to improve tracking behavior [20–22].

Another important research direction is disturbance rejection. Boundary-layer techniques, modified reaching laws, and higher-order sliding modes can alleviate some of the difficulties encountered in conventional switching control [23–25]. Disturbance observers instead estimate unknown effects for compensation, potentially reducing the need for large switching gains [26–33]. Meanwhile, fuzzy logic and neural-network methods have been applied to cope with nonlinearities and uncertain parameters [34–38]. Such intelligent mechanisms offer opportunities for online adjustment, although the interaction between adaptive parameters and robust control dynamics must be considered.

Fractional-order (FO) control provides history-dependent operators and additional design parameters that extend conventional integer-order designs [39–43]. Fractional-order terminal sliding mode controllers have shown promise for manipulator tracking under uncertainty [44,45], and recent work has combined fractional-order sliding control with adaptive fuzzy mechanisms and neural-network observation [46]. These developments suggest potential advantages from coordinating disturbance estimation, fractional-order sliding dynamics, and online gain adjustment. At the same time, a combination of established components alone does not establish novelty; the particular observer structure, sliding-surface formulation, and stability properties must be distinguished from related composite designs.

Motivated by these considerations, this work investigates a Fuzzy-PID–Enhanced Fractional-Order Terminal Sliding Mode Control (Fuzzy PID-FOTSMC) strategy with an Improved Fractional-Order Disturbance Observer (IFODOB) for a planar two-degree-of-freedom manipulator. The objective is to improve disturbance estimation and trajectory tracking under lumped uncertainties while accounting for the effects of time-varying PID gains in the stability analysis. The closely related studies, technical differences, research gaps, and contributions are discussed in Section 2.

The remainder of this paper is organized as follows. Section 2 critically reviews related work and identifies the research gaps and main contributions. Section 3 presents the manipulator dynamics and mathematical preliminaries. Section 4 develops the observer–controller framework and stability analysis. Section 5 reports comparative simulations and ablation studies, and Section 6 concludes the paper.

2. Related Work

This section compares representative studies on fractional-order terminal sliding mode control, disturbance-observer-based compensation, and intelligent adaptive control, focusing on their technical differences and the remaining research questions.

2.1. Fractional-Order Terminal Sliding Mode Control

Wang et al. [39] investigated continuous fractional-order nonsingular terminal sliding mode control for robotic manipulator tracking. Chaudhary and Kumar [44] developed

a fractional-order fast terminal sliding mode scheme under uncertainties and external disturbances. Yao et al. [45] combined fractional-order nonsingular terminal sliding mode control with an RBF neural network for a cable-driven aerial manipulator. These approaches differ in sliding-surface design and uncertainty compensation.

Yang et al. [46] integrated adaptive fuzzy fractional-order nonsingular fast terminal sliding mode control with neural-network-based observation for ultra-precision stages. This closely related study shows that combining fuzzy adaptation, fractional-order sliding control, and observation is not itself new. In contrast, the present work examines a fractional-order PID-type terminal sliding surface with fuzzy-adjusted PID gains, coupled to an improved fractional-order disturbance observer; the resulting time-varying gains and residual observer errors are considered in stability analysis.

2.2. Disturbance Observer-Based Compensation

Existing observer-based approaches include adaptive disturbance-observer-based tracking [26], robust state and disturbance estimation [27], and sliding-mode designs with disturbance observers [30–32]. Qiao et al. [29] addressed multiple disturbances in a space manipulator. These methods employ different estimation and compensation mechanisms; estimation transients are especially relevant to fast terminal tracking.

Alyoussef and Kaya [33] combined adaptive dynamic nonsingular terminal sliding mode control with a fractional disturbance observer, establishing an important precedent for observer–controller integration. The present framework instead couples an IFODOB with a fuzzy-adjusted fractional-order PID-type sliding surface. Its observer performance is evaluated against a selected conventional FODOB under the specified simulation conditions.

2.3. Intelligent and Adaptive Composite Control

Wang et al. [37] developed adaptive fuzzy control with disturbance observers for underwater vehicle–manipulator systems. Lin et al. [47] used neural-network-based robust terminal sliding mode control for quadrotors, while Yang et al. [38] addressed uncertain manipulator dynamics using neural-network adaptation. Composite fractional-order schemes in [45,46] further demonstrate intelligent compensation and adaptation. Unlike these particular designs, the present study directly adjusts proportional, integral, and derivative gains of a fractional-order terminal sliding surface while applying IFODOB feedforward compensation. Its analysis accounts for gain-rate effects and residual estimation errors.

Taken together, these studies demonstrate the effectiveness of intelligent adaptation and composite compensation strategies, while differing in their control architectures, parameter-adjustment mechanisms, and disturbance-estimation approaches. Table 1 summarizes representative related studies in terms of their control strategies and key technical features, highlighting the distinctions between existing approaches and the proposed method.

Table 1. Comparison of representative related studies and the present method.

Reference	Control Approach	Key Technical Features
Wang et al. [39]	Continuous fractional-order nonsingular terminal SMC	Combines a continuous fractional-order nonsingular terminal sliding surface with time-delay estimation (TDE)
Alyoussef and Kaya [33]	Adaptive dynamic nonsingular terminal SMC with fractional disturbance observer	Employs a dynamic nonsingular terminal sliding surface, an adaptive reaching law, and a fractional disturbance observer

Table 1. *Cont.*

Reference	Control Approach	Key Technical Features
Wang et al. [37]	Adaptive fuzzy control with disturbance observers	Uses fuzzy systems to approximate uncertain dynamics and fuzzy observers with dead-zone compensation
Chaudhary and Kumar [44]	Fractional-order fast terminal SMC	Combines a fractional-order fast terminal sliding surface with RBF neural-network approximation and adaptive uncertainty compensation
Yao et al. [45]	Fractional-order nonsingular terminal SMC with RBFNN	Employs fractional-order nonsingular terminal SMC with RBF neural-network disturbance compensation and a power-function switching term
Yang et al. [46]	Adaptive fuzzy FO terminal SMC with neural-network observation	Combines a fractional-order nonsingular fast terminal sliding surface, adaptive fuzzy gain compensation, and neural-network observation
This study	Fuzzy PID-FOTSMC with IFODOB	Develops a fuzzy-adjusted fractional-order PID-type terminal sliding surface and an IFODOB incorporating acceleration estimation error, with stability analysis accounting for time-varying gains and observer errors.

2.4. Research Gaps and Main Contributions

Despite significant advances in fractional-order sliding mode control, adaptive fuzzy control, and disturbance observation, several challenges remain in robotic manipulator trajectory tracking under uncertainties. These include the relatively slow transient response of conventional disturbance observers, the difficulty of balancing convergence speed and steady-state tracking accuracy, and the influence of time-varying control gains and residual disturbance-estimation errors on closed-loop stability.

To address these challenges, the main contributions of this study are summarized as follows:

(1) Improved fractional-order disturbance observer: To enhance disturbance-estimation performance, an improved fractional-order disturbance observer (IFODOB) is developed by introducing acceleration estimation error into the fractional-order correction mechanism while retaining nonlinear velocity-error feedback. Compared with the conventional FODOB, the proposed observer reduces the estimation convergence times from 1.20 s and 1.30 s to 0.26 s and 0.27 s for Joints 1 and 2, respectively, while reducing the steady-state estimation-error bound from ± 0.15 N·m to ± 0.03 N·m under the tested conditions.

(2) Fuzzy-adaptive fractional-order PID-type terminal sliding control: To improve convergence speed and tracking accuracy, a fractional-order PID-type terminal sliding surface is constructed by incorporating nonlinear proportional feedback, fractional-order differentiation, and fractional-order integration, with the corresponding gains adaptively adjusted through fuzzy inference. Comparative simulations demonstrate that the proposed controller achieves position-tracking convergence times of 0.223 s and 0.556 s for Joints 1 and

2, respectively, outperforming three representative benchmark controllers. Ablation studies further verify the contributions of fuzzy gain adaptation and fractional-order dynamics.

(3) Stability analysis incorporating adaptive gain and observer-error effects: To account for the effects of time-varying fuzzy PID gains and residual disturbance-estimation errors, these terms are explicitly considered in the Lyapunov-based stability analysis. Practical finite-time convergence is established under the stated assumptions, while comparative and ablation simulations provide supporting evidence of the proposed framework's tracking and disturbance-compensation performance.

The contributions of this study therefore lie in the specific observer correction mechanism, the fuzzy-adaptive fractional-order PID-type sliding surface, and the corresponding stability analysis, rather than in the individual use of established control techniques.

3. Technical Background

3.1. Manipulator Dynamic Model

For trajectory tracking of n-DOF manipulators, accurate dynamic modeling provides the foundation for both control-law design and disturbance compensation. The Euler–Lagrange formulation is commonly adopted to describe manipulator dynamics and to derive control laws that improve tracking accuracy and disturbance rejection. The Euler–Lagrange equation for an n-DOF manipulator is given as follows:

$$M(q)\ddot{q} + C(q,\dot{q})\dot{q} + F_d\dot{q} + F_s(\dot{q}) + g(q) = \tau \tag{1}$$

where $q, \dot{q}, \ddot{q} \in \mathbb{R}^n$ denote the joint position, velocity, and acceleration vectors, respectively. $M(q) \in \mathbb{R}^{n\times n}$, $C(q,\dot{q}) \in \mathbb{R}^{n\times n}$ and $g(q) \in \mathbb{R}^n$ denote the positive-definite inertia matrix, the Coriolis and centrifugal force matrix and the gravity vector, respectively. $F_d \in \mathbb{R}^{n\times n}$ and $F_s(\dot{q}) \in \mathbb{R}^n$ denote dynamic friction and static friction, respectively. $\tau \in \mathbb{R}^n$ denotes the torques applied at the joints.

In practice, however, obtaining a perfectly accurate dynamic model is difficult. Dynamic parameters are often hard to identify precisely, while external disturbances and unmodeled effects inevitably introduce modeling errors. Considering these uncertainties, the nominal dynamic model of the robotic manipulator is expressed as (2):

$$(M_0 + \Delta M)\ddot{q} + (C_0 + \Delta C)\dot{q} + F_d\dot{q} + F_s(\dot{q}) + g_0 + \Delta g = \tau \tag{2}$$

where $M_0(q)$, $C_0(q,\dot{q})$, and $g_0(q)$ denote nominal parameters of $M(q)$, $C(q,\dot{q})$ and $g(q)$, and the model errors are defined as $\Delta M = M - M_0$, $\Delta C = C - C_0$ and $\Delta g = g - g_0$.

To simplify the model, parameter uncertainties and friction are lumped into a disturbance term $\tau_d(q,\dot{q})$, which is defined as

$$\tau_d(q,\dot{q}) = \Delta M(q)\ddot{q} + \Delta C(q,\dot{q})\dot{q} + \Delta G(q) + F_d\dot{q} + F_s(\dot{q}) \tag{3}$$

By substituting the lumped disturbance defined in Equation (3) into Equation (2), the manipulator dynamics can be rewritten in terms of the nominal model as follows:

$$\tau = M_0(q)\ddot{q} + C_0(q,\dot{q})\dot{q} + g_0(q) + \tau_d(q,\dot{q}) \tag{4}$$

For subsequent analysis, following the approach presented in [48], the explicit algebraic representation of the joint accelerations for a general n-DOF rigid robotic manipulator is directly derived from Equation (1) as follows:

$$\ddot{q} = M^{-1}(q)(\tau - C(q,\dot{q})\dot{q} - F_d\dot{q} - F_s(\dot{q}) - g(q)) \tag{5}$$

3.2. Mathematical Preliminaries

This subsection introduces the fractional-calculus definitions, finite-time convergence lemmas, and assumptions required for the subsequent observer and controller designs.

Definition 1. *According to refs. [49,50], the fractional derivative and integral of β_{th}- order for a function $f(t)$, with terminal value a, are defined in the Riemann–Liouville sense, where the explicit closed-form evaluation depends on the specific form of the function:*

$$ {}_aD_t^{\beta} f(t) = \frac{1}{\Gamma(n-\beta)} \frac{d^n}{dt^n} \int_a^t (t-\tau)^{n-\beta-1} f(\tau) d\tau \tag{6} $$

$$ {}_aI_t^{\beta} f(t) = \frac{1}{\Gamma(\beta)} \int_a^t (t-\tau)^{\beta-1} f(\tau) d\tau \tag{7} $$

where $n-1 < \beta < n$, while D^{β} and I^{β} represent the fractional derivative and integral, respectively. Here, $\Gamma(\beta)$ refers to Euler's Gamma function, expressed as:

$$ \Gamma(\beta) = \int_0^{+\infty} t^{\beta-1} e^{-t} dt \tag{8} $$

In this study, the fractional-order differentiation and integration operators are defined in the Riemann–Liouville sense, with the lower terminal set to the initial time t_0. Unless otherwise specified, these definitions are consistently adopted in the subsequent observer and controller formulations.

Lemma 1. *Under the appropriate regularity conditions, the n_{th} integer-order derivative of the Riemann–Liouville fractional derivative of order β can be expressed as follows [49]:*

$$ \frac{\mathrm{d}^n}{\mathrm{d}t^n} \left({}_aD_t^{\beta} f(t) \right) = {}_aD_t^{\beta+n} f(t) \tag{9} $$

Lemma 2. *According to ref. [51], for a Lyapunov function $\mathcal{V}(t)$ with initial condition $\mathcal{V}(t_0)$, finite-time stability can be determined by the following inequality:*

$$ \dot{\mathcal{V}}(t) \leq -n\mathcal{V}^p(t), \forall t \geq t_0, \mathcal{V}(t_0) \geq 0 \tag{10} $$

where $n > 0$ and $0 < p < 1$. Therefore, the finite convergence time t_f can be formulated as:

$$ t_f \leq \frac{1}{n(1-p)} \mathcal{V}^{1-p}(t_0) \tag{11} $$

Lemma 3. ([50]). *Consider $\mathcal{R}(\nu)$ as the real component of ν, the operators for fractional integration, I_{a+}^{ν} and I_{b-}^{ν}, where $\mathcal{R}(\nu) > 0$, are bounded within the space $L_p(a,b)$, $1 \leq p \leq \infty$. Specifically, this means that $\| I_{a+}^{\nu} f(x) \|_p \leq K \| f(x) \|, \| I_{b-}^{\nu} f(x) \|_p \leq K \| f(x) \|$, where $K = \frac{(b-a)^{\mathcal{R}(\nu)}}{\mathcal{R}(\nu)|\Gamma(\nu)|}$.*

Assumption 1. *The lumped disturbance τ_d is continuous and absolutely continuous with respect to time, and its first-order time derivative exists almost everywhere and is bounded, i.e., $\left|\dot{d}(t)\right| \leq \overline{d}_1$, where $\overline{d}_1 > 0$ is a known constant. Furthermore, the lumped disturbance is bounded, satisfying $|d(t)| \leq \overline{d}_0$, where $\overline{d}_0 > 0$ is a known constant.*

Assumption 2. *The time-varying PID gains $K_p(t)$, $K_i(t)$, and $K_d(t)$, generated by the fuzzy adaptation mechanism, remain positive and bounded, and their time derivatives are bounded. Furthermore, the fractional-order terms involved in the sliding surface and the residual terms associated with the disturbance observer are assumed to be bounded along the considered trajectories.*

4. Proposed Control Methodology

Based on the manipulator dynamic model and mathematical preliminaries presented in Section 3, this section develops the proposed Fuzzy PID-FOTSMC framework integrated with an improved fractional-order disturbance observer (IFODOB). The IFODOB is employed to estimate lumped disturbances and provide feedforward compensation, while a PID-type fractional-order terminal sliding surface is constructed for trajectory tracking. A fuzzy mechanism is further introduced to adaptively adjust the PID gains. The overall control framework is illustrated in Figure 1, and the corresponding stability analysis is provided in the following subsections.

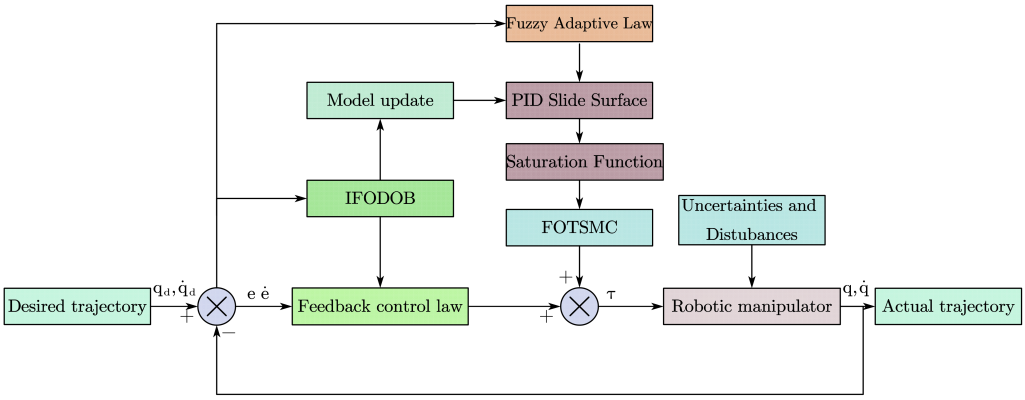


Figure 1. Block diagram of the control system.

As shown in Figure 1, the proposed control framework integrates an improved fractional-order disturbance observer (IFODOB), a PID-type fractional-order terminal sliding surface, and a fuzzy gain-tuning mechanism. The IFODOB estimates the lumped system disturbance, and the estimated disturbance is incorporated into the control law for feedforward compensation. Meanwhile, the fuzzy controller adaptively adjusts the PID gain increments of the sliding surface according to the tracking error and its rate of change. The overall design procedure consists of the following steps.

Step 1: Establish the manipulator model. The dynamic model of the robotic manipulator is formulated, with parameter uncertainties, friction, and external disturbances incorporated into a lumped disturbance term, as described in Section 3.1.

Step 2: Design the disturbance observer. Based on the system state-space representation, the IFODOB is developed to estimate the lumped disturbance. The corresponding observation error dynamics are derived to provide the basis for the subsequent stability analysis.

Step 3: Construct the sliding surface. A PID-type fractional-order terminal sliding surface is defined in terms of the joint tracking error and its fractional-order integral and derivative. The resulting sliding surface provides the foundation for the control-law design.

Step 4: Derive the control law. A reaching law is selected to derive the nominal sliding-mode control law. The estimated disturbance from the IFODOB is then incorporated into the control input to compensate for the effects of uncertainties and external disturbances.

Step 5: Implement fuzzy PID gain tuning. A fuzzy inference system takes the tracking error and its rate of change as inputs and generates PID gain increments for the sliding surface. These increments are used to update the PID gains adaptively, allowing the controller to respond to changing tracking conditions.

Step 6: Verify stability and control performance. Lyapunov-based analysis is conducted to investigate the stability and convergence properties of the disturbance observer and the closed-loop control system under the stated assumptions. Numerical simulations on a planar two-degree-of-freedom robotic manipulator are then performed to evaluate

disturbance-estimation accuracy, trajectory-tracking performance, and control effort. Comparisons with representative baseline controllers and with and without disturbance compensation are used to assess the effectiveness of the proposed design.

4.1. Improved Fractional-Order Disturbance Observer Design

Because robotic manipulator systems are commonly affected by multiple sources of uncertainty, an efficient disturbance observer is crucial for timely estimation and compensation. In this work, an IFODOB is developed to improve disturbance-estimation accuracy, shorten convergence time, and enhance the robustness of the closed-loop tracking system.

The corresponding state-space representation of the system is written as

$$\begin{aligned} \dot{x}_1 &= x_2 \\ \dot{x}_2 &= f(x_1, x_2, t) + u + d \\ \hat{\dot{x}}_2 &= f(x_1, x_2, t) + u + \hat{d} \end{aligned} \tag{12}$$

where $x_1, x_2, \dot{x}_2$ denote system state variables $q, \dot{q}, \ddot{q}$, respectively. Define $\hat{\dot{x}}_2$ and $\hat{x}_2$ as estimates of $\dot{x}_2$ and x_2, respectively. The nonlinear term $f(x_1,x_2,t)$ is calculated from the available joint-position and joint-velocity signals and the nominal dynamic model; it is a known model-based term rather than an independently estimated variable. The control input is $u = M_0^{-1}\tau \in \mathbb{R}^n$. The disturbance term $d = M_0^{-1}\tau_d$ represents the lumped disturbance in the state-space model. Its estimate is denoted by $\hat{d}$, and the corresponding estimation error is defined as $\tilde{d} = d - \hat{d}$.

Under Assumption 1, the state-space disturbance is bounded and satisfies the required regularity conditions for the subsequent observer stability analysis. Furthermore, to estimate and counteract the system's overall uncertainties, the IFODOB is proposed in this paper, whose state-space equations can be written as

$$\begin{aligned} \hat{\dot{x}}_2 &= f(x_1, x_2, t) + u + \hat{d} \\ z &= k_1 \mathrm{sig}(x_2 - \hat{x}_2)^{\alpha} + \mu \\ D^{\beta}\boldsymbol{\mu}(t) &= \boldsymbol{k}_2 \mathrm{sign}(\dot{x}_2 - \hat{\dot{x}}_2) \\ \hat{d} &= \mathbf{z}(\boldsymbol{x}_1, \boldsymbol{x}_2) \end{aligned} \tag{13}$$

where $k_1, k_2 \in \mathbb{R}^{n\times n}$ are positive diagonal matrices, the constant vector $\boldsymbol{\alpha}$ satisfies $0 < \boldsymbol{\alpha} < \mathbf{1}$, and the function sign $(\cdot)$ represents the sign function, where $\mathrm{sig}(\cdot)$ is defined by:

$$\mathrm{sig}(x)^y = \left[|x_1|^{y_1}\mathrm{sign}(x_1), \cdots, |x_n|^{y_n}\mathrm{sign}(x_n)\right]^{\mathrm{T}} \tag{14}$$

The fractional-order observer is formulated with the initial time $t_0 = 0$. The auxiliary fractional-order state is assumed to satisfy the zero-initialization condition $\left[{}_0I_t^{1-\beta}\mu(t)\right]_{t=0^+} = 0$, where $0 < \beta < 1$. The same lower terminal is adopted for the fractional-order operators in the controller. It is worth noting that in the numerical simulations, the joint-acceleration signal is obtained from the manipulator dynamics model. In practical implementations, joint acceleration would need to be measured or estimated using an appropriate method, with measurement noise taken into account.

Compared with the conventional FODOB in [52], the main modification of the proposed IFODOB lies in the error signal employed by the fractional-order correction mechanism. Specifically, the conventional FODOB uses the velocity estimation error, whereas the proposed IFODOB incorporates the acceleration estimation error while retaining nonlinear velocity-error feedback. This modification is intended to enhance the transient response and estimation accuracy of the observer.

Based on the disturbance estimation error $\tilde{d} = d - \hat{d}$, the corresponding observer error dynamics are derived as

$$\dot{\tilde{x}}_2 = \tilde{d} = -k_1 \mathrm{sig}(\tilde{x}_2)^{\alpha} - \mu + d \tag{15}$$

The stability proof is provided in Section 4.4.1.

4.2. PID-FOTSMC Design

To achieve fast and accurate joint-space tracking while maintaining robustness against system uncertainties and external disturbances, a PID-type fractional-order terminal sliding-mode surface is proposed as

$$s = \dot{e} + k_p sig(e)^{r_1} + k_d {}_{t_0}^{E}D_t^{\xi_1}[sig(e)^{r_2}] + k_i {}_{t_0}^{E}I_t^{\xi_2}[sig(e)^{r_3}] \tag{16}$$

where $\boldsymbol{e} = q_{md} - q_m \in \mathbb{R}^n$ represents the control error, with q_{md} and q_m as desired and actual joint positions, respectively. The parameters $\xi_1 \in (0, 1)$ and $\xi_2 \in (0, 1)$ represent the orders of the fractional derivatives and integrals, respectively. The matrices $k_p, k_d, k_i \in \mathbb{R}^{n\times n}$ are positive diagonal time-varying gain matrices adjusted by the fuzzy adaptation mechanism and satisfy Assumption 2. The vectors $r_1, r_2, r_3 \in \mathbb{R}^n$ fulfill the conditions $0 < r_1, r_2, r_3 < 1$.

Under the sliding-mode control law, the tracking error converges to zero along the sliding surface. To facilitate the subsequent control-law design, differentiating the sliding surface then yields

$$\begin{aligned} \dot{s} = \ddot{e} + k_p(t)(\mathrm{sig}(e)^{r_1})' + k_d(t) {}_{t_0}^{E}D_t^{\xi_1+1}[\mathrm{sig}(e)^{r_2}] + k_i(t) {}_{t_0}^{E}I_t^{\xi_2-1}[\mathrm{sig}(e)^{r_3}] \\ + \dot{k}_p(t)\mathrm{sig}(e)^{r_1} + \dot{k}_d(t) {}_{t_0}^{E}D_t^{\xi_1}[\mathrm{sig}(e)^{r_2}] + \dot{k}_i(t) {}_{t_0}^{E}I_t^{\xi_2}[\mathrm{sig}(e)^{r_3}] \end{aligned} \tag{17}$$

The time-varying PID gains introduce an additional term $R_k(t)$, defined as

$$R_k(t) = \dot{k}_p(t)\mathrm{sig}(e)^{r_1} + \dot{k}_d(t) {}_{t_0}^{E}D_t^{\xi_1}[\mathrm{sig}(e)^{r_2}] + \dot{k}_i(t) {}_{t_0}^{E}D_t^{\xi_2}[\mathrm{sig}(e)^{r_3}].$$

According to Assumption 2, this additional term is uniformly bounded, i.e., $|R_k(t)| \le \overline{R}_k$, where $\overline{R}_k$ is a finite nonnegative constant.

To accelerate the reaching process, the reaching law is selected as (18).

$$\dot{s} = -\lambda_1 s - \lambda_2 sig(s)^p \tag{18}$$

where $\lambda_1, \lambda_2 \in \mathbb{R}^{n\times n}$ are positive diagonal constant matrices, and $p \in \mathbb{R}^n$, whose entries lie in $(0, 1)$.

The nominal control law is then obtained as

$$\begin{aligned} &\tau = C_0\dot{q} + G_0 + \tau_d \\ &+M_0(\lambda_1 s + \lambda_2 sig(s)^p) \\ &+M_0\left(\ddot{q}_d + k_p r_1 |e_i|^{r_1-1}\dot{e}_i + k_d D^{\xi+1}[sig(e)^{r_2}] + k_i I_t^{\xi_2-1}[sig(e)^{r_3}]\right) \end{aligned} \tag{19}$$

However, when external disturbances are unknown or load disturbances fluctuate, the effectiveness of SMC can be compromised. To mitigate this issue, IFODOB is utilized to evaluate external disturbances. By incorporating the estimated system disturbance $\hat{\tau}_d$ into (19), the final control law is as

$$\begin{aligned} &\tau = C_0\dot{q} + G_0 + \hat{\tau}_d \\ &+M_0(\lambda_1 s + \lambda_2 sig(s)^p) \\ &+M_0\left(\ddot{q}_d + k_p r_1 |e_i|^{r_1-1}\dot{e}_i + k_d D^{\xi+1}[sig(e)^{r_2}] + k_i I_t^{\xi_2-1}[sig(e)^{r_3}]\right) \end{aligned} \tag{20}$$

4.3. Adaptive Fuzzy Control for PID Gain Tuning

To reduce SMC chattering and further improve trajectory-tracking performance, a fuzzy controller is introduced to adaptively tune the PID gains of the sliding surface. Based on expert knowledge and fuzzy-logic inference, fuzzy control adjusts controller parameters without requiring an exact mathematical model. This feature is particularly suitable for nonlinear robotic systems subject to model uncertainties and external disturbances. Owing to its adaptability and robustness, fuzzy control has been widely used in industrial automation, robotics, and intelligent transportation.

The proposed fuzzy controller dynamically adjusts the PID gains on the sliding surface. The inputs are the angle error e and its rate of change $\dot{e}$, while the outputs are the gain increments Δk_p, Δk_i and Δk_d. The input domains of e and ė are limited to $[-0.1, 0.1]$ and partitioned into seven fuzzy sets: negative big (NB), negative medium (NM), negative small (NS), zero (ZO), positive small (PS), positive medium (PM), and positive big (PB). Correspondingly, the output ranges for Δk_p, Δk_i and Δk_d are set to $[-4, 4]$, $[-2, 2]$, and $[-2, 2]$, respectively, each spanning the same seven fuzzy sets. Triangular membership functions are used to fuzzify e, $\dot{e}$, and the outputs Δk_p, Δk_i and Δk_d, as illustrated in Figure 2.

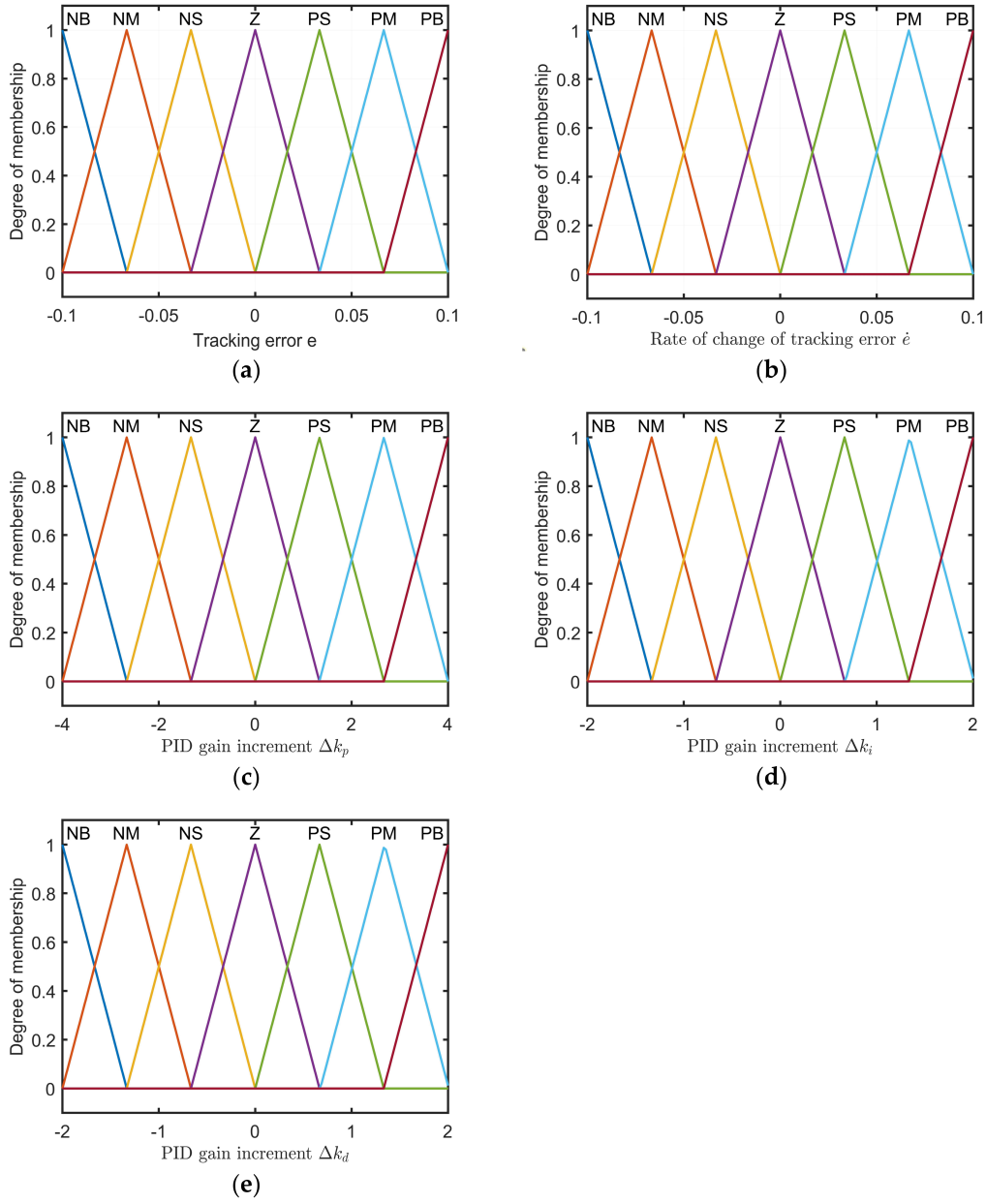


Figure 2. Membership functions of the proposed fuzzy controller: (**a**) input variable, tracking error e; (**b**) input variable, rate of change of tracking error $\dot{e}$; (**c**) output variable, proportional gain increment Δk_p; (**d**) output variable, integral gain increment Δk_i; and (**e**) output variable, derivative gain increment Δk_d.

Fuzzy rules are generally selected based on empirical observations or expert experience to improve system stability. Table 2 shows the fuzzy control rules for adjusting Δk_p, Δk_i and Δk_d, while Figure 3 illustrates the characteristic surfaces of the three fuzzy gain increments.

Although they share the same input variables and linguistic terms, their surfaces exhibit different characteristics due to their distinct control objectives. Specifically, Δk_p primarily accelerates error convergence, while Δk_d enhances system damping to suppress overshoot and oscillations.

Table 2. Rule matrix of supervisory fuzzy control.

$\Delta k_p \Delta k_i \Delta k_d$	$\dot{e}$						
e	**NB**	**NM**	**NS**	**ZO**	**PS**	**PM**	**PB**
NB	PB/NB/PM	PB/NB/PS	PM/NM/ZO	PM/ZO/ZO	PS/NM/PM	ZO/NB/PB	NS/NB/PB
NM	PB/NB/PM	PM/NM/PS	PM/NS/ZO	PM/PS/ZO	PS/NS/PM	ZO/NM/PB	NS/NB/PB
NS	PM/NB/PS	PM/NS/ZO	PS/PS/ZO	ZO/PM/ZO	NS/PS/PM	NM/NS/PB	NB/NB/PB
ZO	NS/NB/PB	ZO/NM/PM	ZO/NS/PS	ZO/ZO/ZO	ZO/NS/PS	ZO/NM/PM	NS/NB/PB
PS	NB/NB/PB	NM/NS/PB	NS/PS/PM	ZO/PM/ZO	PS/PS/ZO	PM/NS/ZO	PM/NB/PS
PM	NS/NB/PB	ZO/NM/PB	PS/NS/PM	PM/PS/ZO	PM/NS/ZO	PM/NM/PS	PB/NB/PM
PB	NS/NB/PB	ZO/NB/PB	PS/NM/PM	PM/ZO/ZO	PM/NM/ZO	PB/NB/PS	PB/NB/PM

Note: Each entry in the rule matrix represents the linguistic output values of Δk_p, Δk_i and Δk_d, in that order. The row and column indices correspond to the fuzzy linguistic terms of the two input variables, e and $\dot{e}$, respectively.

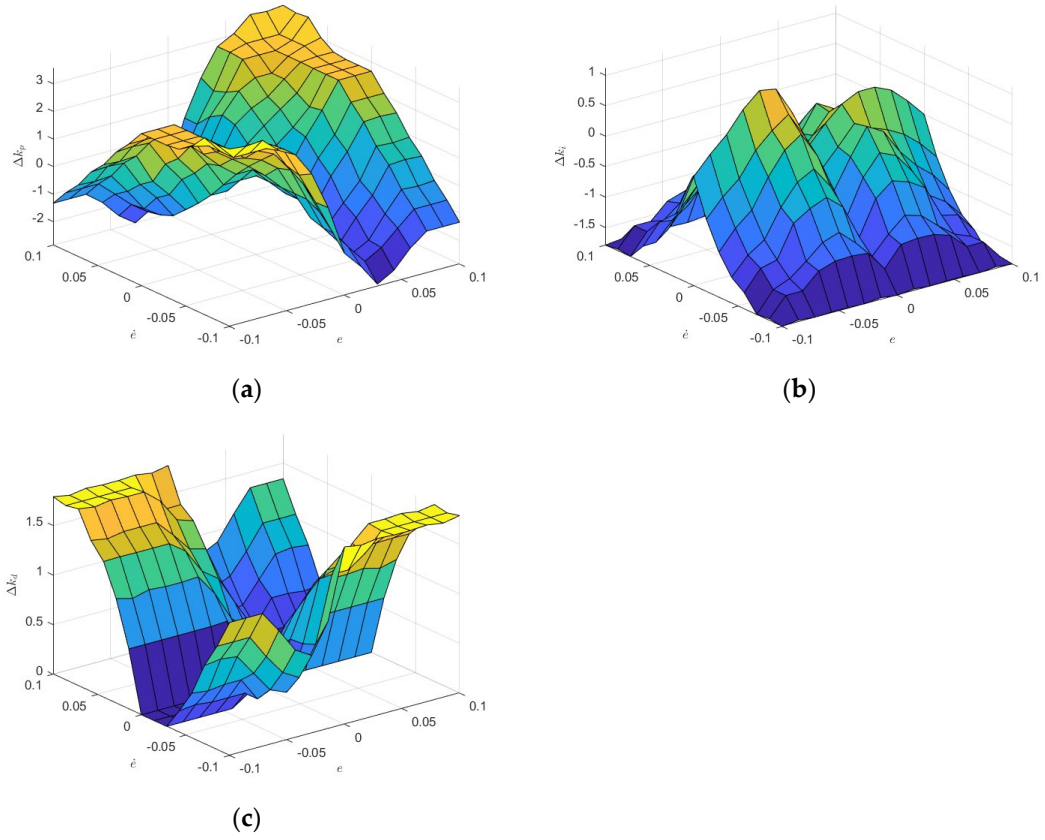


Figure 3. Characteristic surface of the fuzzy inference system: (**a**) proportional gain increment Δk_p; (**b**) integral gain increment Δk_i; (**c**) derivative gain increment Δk_d.

Notably, the surface of Δk_i exhibits two distinct positive peak regions, which result from the specific design of the integral gain adjustment rules. Since integral action primarily eliminates persistent tracking errors and improves steady-state accuracy, positive Δk_i increments are assigned to small positive and negative errors with nearly zero error rates. In contrast, zero or negative increments are assigned to the equilibrium point and rapid transient conditions, respectively, to prevent unnecessary gain adjustments and excessive

integral accumulation. Furthermore, the approximately symmetric distribution of the Δk_i rules ensure consistent gain adaptation for positive and negative tracking errors. This distinct surface reflects the different role of integral gain adaptation and contributes to balancing transient response, overshoot suppression, and steady-state tracking accuracy.

4.4. Stability Analysis

4.4.1. Observer Stability Analysis

Proof: Based on the disturbance estimation error $\tilde{d} = d - \hat{d}$, the Lyapunov function is defined as $V_1 = \frac{1}{2}\tilde{d}^T\tilde{d}$ to analyze the stability of the disturbance observer. By combining Equation (15), the derivative of this function can be expressed as

$$\begin{aligned}
\dot{V}_1 &= \tilde{d}\dot{\tilde{d}} \\
&= \tilde{d}\left(d - k_1 \mathrm{sig}(\tilde{x}_2)^{\alpha} - \mu\right)' \\
&= \tilde{d}\left(d - k_1 \mathrm{sig}(\tilde{x}_2)^{\alpha} - k_2 t_0 I_t^{\beta}\mathrm{sign}(\dot{x}_2 - \hat{\dot{x}}_2)\right)' \\
&= \tilde{d}\left(\dot{d} - k_1\alpha \mathrm{sig}(\tilde{x}_2)^{\alpha-1}\dot{\tilde{x}}_2 - k_2 t_0 I_t^{\beta-1}\mathrm{sign}(\dot{x}_2 - \hat{\dot{x}}_2)\right)' \\
&= \tilde{d}\left(\dot{d} - k_1\alpha \mid \tilde{x}_2 \mid^{\alpha-1}\tilde{d} - k_2 t_0 I_t^{\beta-1}\mathrm{sign}\left(\tilde{d}\right)\right) \\
&= -k_1\alpha \mid \tilde{x}_2 \mid^{\alpha-1}\tilde{d}^2 + \tilde{d}\left(\dot{d} - k_2 t_0 D_t^{1-\beta}\mathrm{sign}\left(\tilde{d}\right)\right)
\end{aligned} \tag{21}$$

According to Assumption 1, the disturbance-related terms are bounded. For the observer stability analysis, it is further assumed that the observer parameters and the disturbance-related fractional-order term satisfy $\tilde{d}\left(\dot{d} - k_{2_{t_0}} D_t^{1-\beta}\mathrm{sign}\left(\tilde{d}\right)\right) \le 0$. Under this additional sufficient condition, Equation (21) can be bounded as follows:

$$\dot{V}_1 \le -k_1\alpha \mid \tilde{x}_2 \mid^{\alpha-1}\tilde{d}^2 \le 0 \tag{22}$$

It follows from Equation (22) that the observer is Lyapunov stable under the stated conditions. Furthermore, assume that the coefficient of V_1(V_1) admits a positive lower bound in the considered operating region, satisfying $2k_1\alpha\left|\tilde{x}_2\right|^{\alpha-1} \ge c > 0$. Then, substituting $\tilde{d}^2 = 2V_1$ into Equation (22) yields Equation (23), and consequently, $\dot{V}_1 \le -cV_1$

$$\dot{V}_1 \le -2k_1\alpha \mid \tilde{x}_2 \mid^{\alpha-1} V_1 \tag{23}$$

For a small threshold ϵ_1, the convergence time can be obtained as

$$t_f \le \max\left\{0, \frac{1}{c}\ln\left(\frac{V_1(0)}{\epsilon_1}\right)\right\} \tag{24}$$

The above derivation shows that the disturbance-estimation error converges to a prescribed neighborhood of the origin within finite time under the stated conditions. Specifically, for any prescribed disturbance-estimation accuracy $\varepsilon_d > 0$, we choose the Lyapunov function threshold as $\varepsilon_1 = \varepsilon_d^2/2$. According to Equation (24), there exists a finite time t_f such that $V_1(t) \le \varepsilon_1$ for all $t \ge t_f$. Since $V_1 = \frac{1}{2}\left|\tilde{d}\right|^2$, it follows that the disturbance-estimation error satisfies $\left|d - \hat{d}\right| = \left|\tilde{d}\right| \le \varepsilon_d, \forall t \ge t_f$. Thus, the observer achieves practical finite-time convergence to a prescribed neighborhood of the origin.

4.4.2. Controller Stability Analysis

To investigate the closed-loop stability, consider the Lyapunov function $V_2 = \frac{1}{2}s^2$. In the ideal case without disturbance-estimation errors and fuzzy gain-rate effects, its derivative can be expressed as

$$\dot{V}_2 = -s^{\mathrm{T}}\lambda_1 s - s^{\mathrm{T}}\lambda_2 \mathrm{sig}(s)^p \tag{25}$$

Considering both the disturbance-estimation error and the additional term $R_k(t)$ induced by the time-varying fuzzy PID gains, the derivative of the Lyapunov function satisfies

$$\begin{aligned}\dot{V}_2 &= -s^T\lambda_1 s - s^T\lambda_2 \mathrm{sig}(s)^p + s^T\left(\hat{d}-d\right) + s^T R_k(t) \\ &\le -\left(\lambda_{1,\min}\parallel s \parallel -\epsilon_{\mathrm{eff}}\right)\parallel s \parallel -\lambda_{2,\min}\parallel s \parallel^{p+1}\end{aligned} \tag{26}$$

where $\lambda_{1,min}$ and $\lambda_{2,min}$ represent the minimum eigenvalues of matrices λ_1 and λ_2, respectively. $\epsilon_{\mathrm{eff}} = \epsilon + \overline{R}_k$ denotes the effective uncertainty bound, which includes both the disturbance-estimation error and the additional effect of the time-varying fuzzy PID gains. Substituting $s = \left(2V_2\right)^{\frac{1}{2}}$, we obtain

$$\dot{V}_2 \le -\left(\lambda_{1,\min}\parallel s \parallel -\epsilon_{\mathrm{eff}}\right)\parallel s \parallel -\overline{\lambda}_{2,\min} V_2^{(1+p)/2} \tag{27}$$

where $\lambda_{2,\min} = 2^{\frac{1+p}{2}}\lambda_{2,\min}$. When $|s| \ge \epsilon_{\mathrm{eff}}/\lambda_{1,\min}$, the previous inequality can be simplified as

$$\dot{V}_2 \le -\overline{\lambda}_{2,min} V_2^{\frac{1+p}{2}} \tag{28}$$

According to Lemma 2, the sliding variable s converges to the prescribed neighborhood $|s| \le \delta_{s1} = \epsilon_{\mathrm{eff}}/\lambda_{1,\min}$ within a finite time T_{r1}, whose upper bound is given by

$$T_{r1} = \frac{1}{\overline{\lambda}_{2,min}\left(1-\frac{1+p}{2}\right)}\left(V_2^{1-\frac{1+p}{2}}(\mathbf{s}_0) - V_2^{1-\frac{1+p}{2}}(\mathbf{s}_1)\right) \tag{29}$$

where $V_2(s_0)$ and $V_2(s_1)$ denote the values at the initial state and at the convergence accuracy δ_{s1}, respectively.

Similarly, we obtain

$$\dot{V}_2 \le -2\lambda_{1,\min} V_2, \parallel s \parallel \ge \ \delta_{s2} \tag{30}$$

where $\delta_{s2} = \left(\frac{\epsilon_{\mathrm{eff}}}{\lambda_{2,\min}}\right)^{1/p}$.

It follows that s will converge to the neighborhood $\parallel s \parallel \le \left(\frac{\epsilon}{\lambda_{2,min}}\right)^{1/p} = \delta_{s2}$ within a finite time T_{r2}, with T_{r2} given by.

Therefore, the sliding variable enters the neighborhood $|s| \le \delta_{s2} = \left(\epsilon_{\mathrm{eff}}/\lambda_{2,\min}\right)^{1/p}$ within finite time. From Equation (30), the corresponding convergence time is bounded by

$$T_{r2} \le \max\left\{0, \frac{1}{\lambda_{1,\min}}\ln\left(\frac{\parallel s(0) \parallel}{\delta_{s2}}\right)\right\} \tag{31}$$

Here, $V_2(s_2)$ denotes $V_2(s)$ evaluated at δ_{s2}.

Under control law (20), when the disturbance-estimation error and the fuzzy gain-rate-dependent term satisfy the stated boundedness conditions, the sliding variable converges to the neighborhood $|s| \le \delta_s = \min(\delta_{s1}, \delta_{s2})$ within finite time. A conservative upper bound of the reaching time is given by $T_r = \max\{T_{r1}, T_{r2}\}$. Substituting the sliding surface tracking error obtained from the above analysis into Equation (14), we can rewrite the expression as

$$\dot{e} = -k_p \mathrm{sig}(e)^{r_1} - k_d {}_{t_0}^{E}D_t^{\xi_1}[\mathrm{sig}(e)^{r_2}] - \left(k_i - \frac{s}{{}_{t_0}^{E}I_t^{\xi_2}[\mathrm{sig}(e)^{r_3}]}\right){}_{t_0}^{E}I_t^{\xi_2}[\mathrm{sig}(e)^{r_3}] \tag{32}$$

When $k_i - \frac{s}{{}_{t_0}^{E}I_t^{\xi_2}[\mathrm{sig}(e)^{r_3}]} \ge 0$, this expression ensures that the tracking error can converge eventually to the equilibrium point along the desired FONTSM surface within a finite time, and the final equilibrium point e will necessarily satisfy $k_i - \frac{s}{{}_{t_0}^{E}I_t^{\xi_2}[\mathrm{sig}(e)^{r_3}]} \le 0$:

$${}_{t_0}^{E}I_t^{\xi_2}[\mathrm{sig}(e)^{r_3}] \le \frac{s}{k_i} \tag{33}$$

Combining this with $|s_i| \le \delta_s$, we obtain:

$$\left|{}_{t_0}^{E}I_t^{\xi_2}[\mathrm{sig}(e)^{r_3}]\right| \le \frac{s}{k_i} \le \frac{\delta_s}{k_i} \tag{34}$$

This demonstrates the achievable upper bound of the tracking error e. Moreover, by applying Lemma 3 and setting $p = \infty$, we derive the following result:

$$\left|{}_{t_0}^{E}I_t^{\xi_2}[\mathrm{sig}(e)^{r_3}]\right| \le K_i|e_i|_{max}^{b_i} \tag{35}$$

where $|e_i|_{max}^{b_i}$ denotes the maximum value of $|e_i|^{b_i}$. Subsequently, we select a time-varying parameter $\sigma_{\mathrm{i}} \ge 1$, ensuring it satisfies the following condition:

$$\left|{}_{t_0}^{E}I_t^{\xi_2}[\mathrm{sig}(e)^{r_3}]\right| = \frac{K_i|e_i|_{max}^{b_i}}{\sigma_{\mathrm{i}}} \tag{36}$$

Combining this result with Equation (34) gives:

$$\frac{K_i|e_i|_{max}^{b_i}}{\sigma_{\mathrm{i}}} \le \frac{\delta_s}{k_i} \tag{37}$$

Thus, the tracking-error convergence accuracy can be obtained as

$$|e_i| \le |e_i|_{max} \le \left(\frac{\sigma_i\delta_s}{K_ic_2}\right)^{\frac{1}{b_i}} = \delta_e \tag{38}$$

To estimate the convergence time, let $V_3 = \frac{1}{2}e^2$. Referring to Equation (32), the derivative of V_3 yields

$$\begin{aligned} \dot{V}_3 &= e\dot{e} \\ &= e\Big(-k_p\mathrm{sig}(e)^{r_1} - k_{d}{}_{t_0}^{E}D_t^{\xi_1}[\mathrm{sig}(e)^{r_2}] - \Big(k_i - \tfrac{s}{t-t_0}I_t^{\xi_2}[\mathrm{sig}(e)^{r_3}]\Big){}_{t_0}^{E}I_t^{\xi_2}[\mathrm{sig}(e)^{r_3}]\Big) \\ &\le -k_p e\mathrm{sig}(e)^{r_1} \\ &\le -k_p 2^{\frac{r_1+1}{2}}V_3^{\frac{r_1+1}{2}} \end{aligned} \tag{39}$$

Lemma 2 ensures that the tracking error converges to within δ_x in no more than T_e; that is,

$$T_e = \frac{1}{2^{\frac{r_1+1}{2}}k_p(\frac{1-r_1}{2})}\left(V_3^{1-\frac{r_1+1}{2}}(\delta_0) - V_3^{1-\frac{r_1+1}{2}}(\delta_e)\right) \tag{40}$$

where $V_3(\delta_0)$ and $V_3(\delta_e)$ represent $V_3(e)$ evaluated at the initial and at δ_e, respectively. Thus, the tracking error e remains inside the region $|e| < \delta_e$ after the time T_s.

$$T_s = T_e + T_r \tag{41}$$

By substituting (42) into (14), we can obtain the bound of $\dot{e}_i$:

$$\begin{aligned} |\dot{e}_i| &= \left|s - k_p\mathrm{sig}(e)^{r_1} - k_{d}{}_{t_0}^{E}D_t^{\xi_1}[\mathrm{sig}(e)^{r_2}] - k_{i}{}_{t_0}^{E}I_t^{\xi_2}[\mathrm{sig}(e)^{r_3}]\right| \\ &\le \delta_s + k_p\delta_e^{r_1} + k_d\tfrac{\Gamma(r_2+1)}{\Gamma(r_2+1-\xi_1)}\delta_e^{r_2-\xi_1} + k_i\tfrac{\Gamma(r_3+1)}{\Gamma(r_3+1+\xi_1)}\delta_e^{r_3+\xi_2} \end{aligned} \tag{42}$$

According to Lemma 2, the tracking error converges to the prescribed neighborhood $|e| < \delta_e$ within finite time. Therefore, under the stated boundedness and gain conditions, the proposed closed-loop controller achieves practical finite-time convergence, while explicitly accounting for the time-varying fuzzy PID gains.

5. Simulations

Numerical simulations were conducted on a computer equipped with an Intel Core i7-10875H CPU (2.30 GHz) and 32 GB RAM to evaluate the effectiveness and robustness of the proposed control framework for a planar two-degree-of-freedom (2-DOF) robotic manipulator, as illustrated in Figure 4. The simulation study was organized into three main parts, followed by an ablation study. First, the disturbance-estimation performance of the proposed improved fractional-order disturbance observer (IFODOB) was evaluated against that of the conventional fractional-order disturbance observer (FODOB) reported in [52] under identical observer parameters. Second, the trajectory-tracking performance of the proposed Fuzzy PID-FOTSMC was compared with three representative benchmark controllers, namely fractional-order sliding mode (FOSM) [53], fractional-order terminal sliding mode (FOTSM) [43], and fractional-order nonsingular terminal sliding mode (FONTSM) [52], under model uncertainties, friction, and external disturbances. Third, an ablation study was conducted to investigate the individual contributions of fuzzy PID gain adaptation, fractional-order dynamics, and disturbance observer-based compensation to the overall tracking performance.

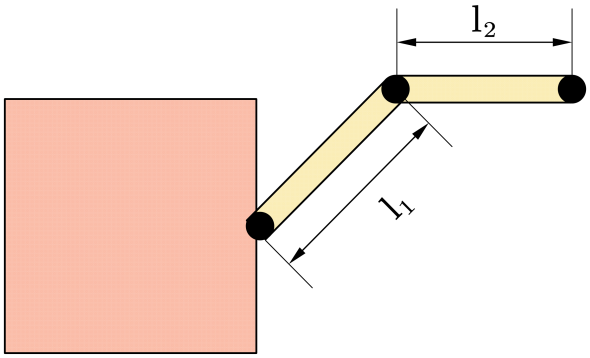


Figure 4. Simulation model of a two-DOF manipulator.

The evaluation considered both transient and steady-state behaviors, including disturbance-estimation convergence, joint-position and angular-velocity tracking errors, convergence time, steady-state mean absolute error (SS-MAE), and maximum absolute control torque. In particular, the convergence time was defined as the earliest time after which the absolute joint-position tracking error remained within 0.002 rad, while the SS-MAE was calculated over the interval of 3–5 s. The disturbance-rejection capability was further examined by comparing the proposed controller with and without IFODOB compensation. The following subsections present the manipulator model, simulation configurations, comparative results, and ablation analysis in detail.

5.1. Simulation Settings

As illustrated in Figure 4, the manipulator system consists of a base and a rigidly mounted arm. Since the base inertia is much larger than that of the manipulator, the system is equivalently modeled as a fixed-base manipulator. The kinematic and dynamic parameters of the manipulator are listed in Table 3.

Table 3. The kinematic and dynamic parameters of the manipulator.

	Mass-m (kg)	**Inertia-I (kg · m^2)**	**Length-l (m)**
Link-1	0.2	0.5	1
Link-2	0.2	1	0.85

The manipulator is initially configured as follows: $q_1(0) = 1$ rad, $\dot{q}_1(0) = 0$ rad/s, $q_2(0) = 1.5$ rad and $\dot{q}_2(0) = 0$ rad/s. The remaining parameter settings are: $k_p' = [4\ 4]^T, k_d' = [2\ 2]^T, k_i' = [2\ 2]^T, \xi_1 = 0.2, \xi_2 = 0.5, r_1 = r_3 = 0.5, r_2 = 0.8$, $\lambda_1 = \lambda_2 = 2, p = 0.5$, $\alpha = 0.8, \beta = 0.9$.

The reference trajectory is defined as:

$$\begin{aligned} q_{1d} &= 0.5sin(3t) + 0.05sin(6t) - 0.2 \\ q_{2d} &= -0.2cos(3 * t) - 0.04sin(6t) - 0.2cos(6t) + 0.6 \end{aligned} \tag{43}$$

The friction and unknown disturbance terms are defined as follows:

$$\tau_d = \left[0.05\dot{q}_1 + sin(3q_1) + 3.05\dot{q}_2 - sin(2q_2) - 2\right]^T \tag{44}$$

It should be noted that Equation (44) defines the total external disturbance considered in the simulations, including friction and unknown external disturbances, but does not account for model parameter uncertainties. According to Equations (2)–(4), model parameter uncertainties and the external disturbances specified in Equation (44) are subsequently combined into a lumped disturbance term for the observer and controller design. The specific simulation settings are provided in Sections 5.2 and 5.3.

5.2. Evaluation of Disturbance Observer

The effectiveness of the IFODOB is evaluated by comparison with the FODOB in [52] under identical observer parameters. To isolate the disturbance-estimation performance of the observers, the nominal dynamic model is assumed to be accurately known in this subsection, i.e., $M_0 = M, C_0 = C$ and $g_0 = g$. Thus, only the friction and unknown external disturbances specified in Equation (44) are considered. The FODOB is expressed as

$$\begin{aligned} \boldsymbol{z} &= \boldsymbol{k}_1 sig(\boldsymbol{x}_2 - \hat{\boldsymbol{x}}_2)^{\boldsymbol{\alpha}} + \boldsymbol{\mu} \\ D^{\beta}\boldsymbol{\mu}(t) &= \boldsymbol{k}_2 sign(\boldsymbol{x}_2 - \hat{\boldsymbol{x}}_2) \\ \hat{\boldsymbol{d}} &= \boldsymbol{z}(\boldsymbol{x}_2, \hat{\boldsymbol{x}}_2) \end{aligned} \tag{45}$$

To further clarify the influence of the modified fractional-order correction mechanism, the proposed IFODOB is compared with the conventional FODOB under identical observer parameters and simulation conditions. As indicated by Equations (13) and (45), the two observers employ different error signals in their fractional-order correction terms. Specifically, the proposed IFODOB incorporates acceleration estimation error, whereas the conventional FODOB employs velocity estimation error. The disturbance-estimation results of the two observers are shown in Figure 5. Figure 5a,b compare the actual disturbances applied to the two manipulator joints with the corresponding observer estimates. Both observers can track the disturbance trend; however, the IFODOB follows the true disturbance more closely. Figure 5c,d further show the estimation errors over time. Specifically, the IFODOB converges within 0.26 s and 0.27 s for Joint 1 and Joint 2, respectively, with a steady-state error bound of ±0.03 N·m. By contrast, the FODOB requires 1.2 s and 1.3 s for the two joints and yields a steady-state error bound of ±0.15 N·m. These results demonstrate that the IFODOB provides substantially faster convergence and higher estimation accuracy, thereby offering a stronger basis for feedforward disturbance compensation.

To further evaluate the contribution of disturbance compensation to trajectory tracking, the Fuzzy PID-FOTSMC with IFODOB compensation is compared with its uncompensated counterpart. Figure 6 presents the joint position and angular-velocity tracking errors, respectively. The uncompensated controller can still keep the tracking errors bounded, but the introduction of IFODOB compensation leads to faster convergence, higher tracking accuracy, and stronger rejection of external disturbances. This comparison confirms that accurate observer-based compensation is a key component of the proposed high-performance tracking framework.

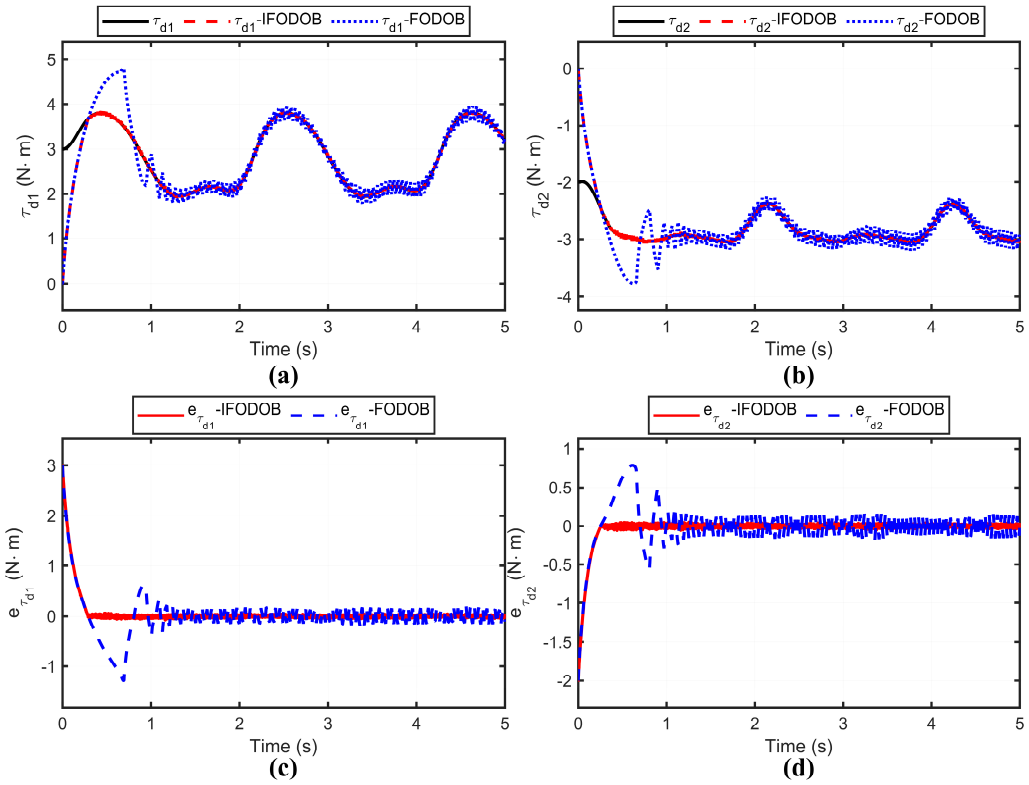


Figure 5. System disturbance estimation results. (**a**) Actual and estimated disturbance of Joint 1. (**b**) Actual and estimated disturbance of Joint 2. (**c**) Estimation error of Joint 1. (**d**) Estimation error of Joint 2.

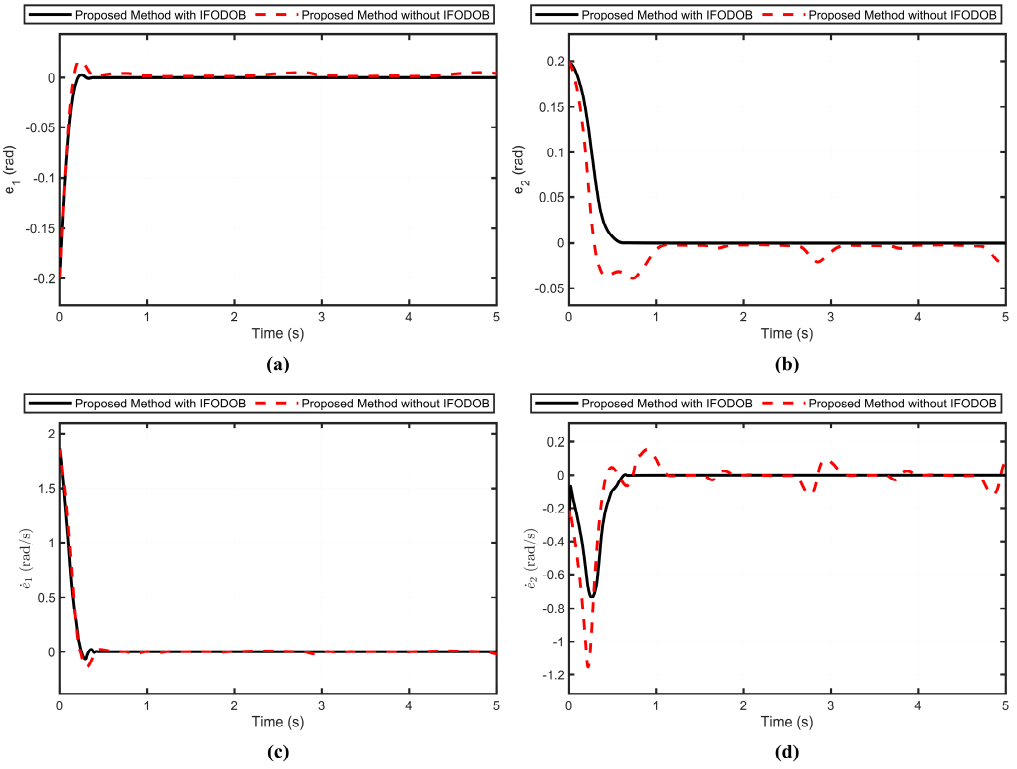


Figure 6. Joint position and angular velocity tracking errors. (**a**) Joint 1 position error. (**b**) Joint 2 position error. (**c**) Joint 1 angular velocity error. (**d**) Joint 2 angular velocity error.

5.3. Evaluation of Control Algorithm

To further evaluate the performance of the proposed control method, it is compared with three representative control algorithms from the literature, namely:

FOTSM proposed in ref. [43]:

$$s = \dot{e} + k'^{E}_{i t_0} I^{\xi}_{t} \left[sig(e)^{b} \right] \tag{46}$$

FOSM proposed in ref. [53]:

$$s = \dot{e} + k'_{p} e + k'^{E}_{i t_0} I^{\xi}_{t} \left[sig(e)^{b} \right] \tag{47}$$

FONTSM proposed in ref. [52]:

$$s = \dot{e} + k'_{p} sig(e)^{r_1} + k'^{E}_{i t_0} I^{\xi_2}_{t} \lfloor sig(e)^{r_3} \rceil \tag{48}$$

To ensure a fair comparison, the parameters of all baseline algorithms are configured consistently with those of the proposed controller. To evaluate the robustness of the control algorithms against model uncertainties, the nominal dynamic parameters are deliberately set as $M_0 = 1.1M$,$C_0 = 0.9C$ and $g_0 = 0.95g$, thereby introducing mismatches between the nominal and actual dynamic models. According to Equations (2)–(4), the resulting model uncertainties, together with the friction and unknown external disturbances specified in Equation (44), are incorporated into the lumped disturbance term. Thus, the overall lumped disturbance accounts for both model parameter uncertainties and external disturbances.

Figure 7 presents the comparative simulation results. Figure 7a–d show the joint position and angular-velocity tracking responses of the proposed algorithm and the baseline controllers. All controllers can follow the desired trajectories and maintain bounded errors, confirming their basic effectiveness. Figure 7e–h further compare the tracking errors in position and angular velocity. Compared with FOTSM, FOSM, and FONTSM, the proposed method achieves faster convergence, smaller steady-state errors, and reduced overshoot. Figure 8 shows the time histories of the control torques. The peak control torques of the four controllers are further compared in Table 4. Although the proposed method requires a slightly higher peak torque for Joint 1, its control effort remains comparable to that of the benchmark controllers.

Table 4. Quantitative performance comparison of different control algorithms.

Joint	Controller	Convergence Time (s)	Steady-State MAE ($\times 10^{-3}$ rad)	Maximum Torque (N·m)
1	Proposed Method	0.223	0.000174	25.544
1	FOSM	0.976	0.000456	24.012
1	FOTSM	2.296	0.331919	20.128
1	FONTSM	1.697	0.008029	20.151
2	Proposed Method	0.556	0.001991	15.178
2	FOSM	1.076	0.013758	16.049
2	FOTSM	1.869	0.223094	13.523
2	FONTSM	1.490	0.007456	15.163

Note: Convergence time is the earliest time after which the absolute joint-position tracking error remains within 0.002 rad. Steady-state MAE is computed over 3–5 s; maximum torque denotes the peak absolute control torque.

To quantitatively evaluate the performance of different control algorithms, three performance indices are considered: convergence time, steady-state mean absolute error (SS-MAE), and maximum absolute control torque. The convergence time characterizes the transient response speed and is defined as the earliest time after which the absolute position tracking error remains within a prescribed tolerance of 0.002 rad. The SS-MAE is calculated over the interval of 3–5 s to evaluate steady-state tracking accuracy, while the maximum absolute control torque reflects the peak control input required by each algorithm.

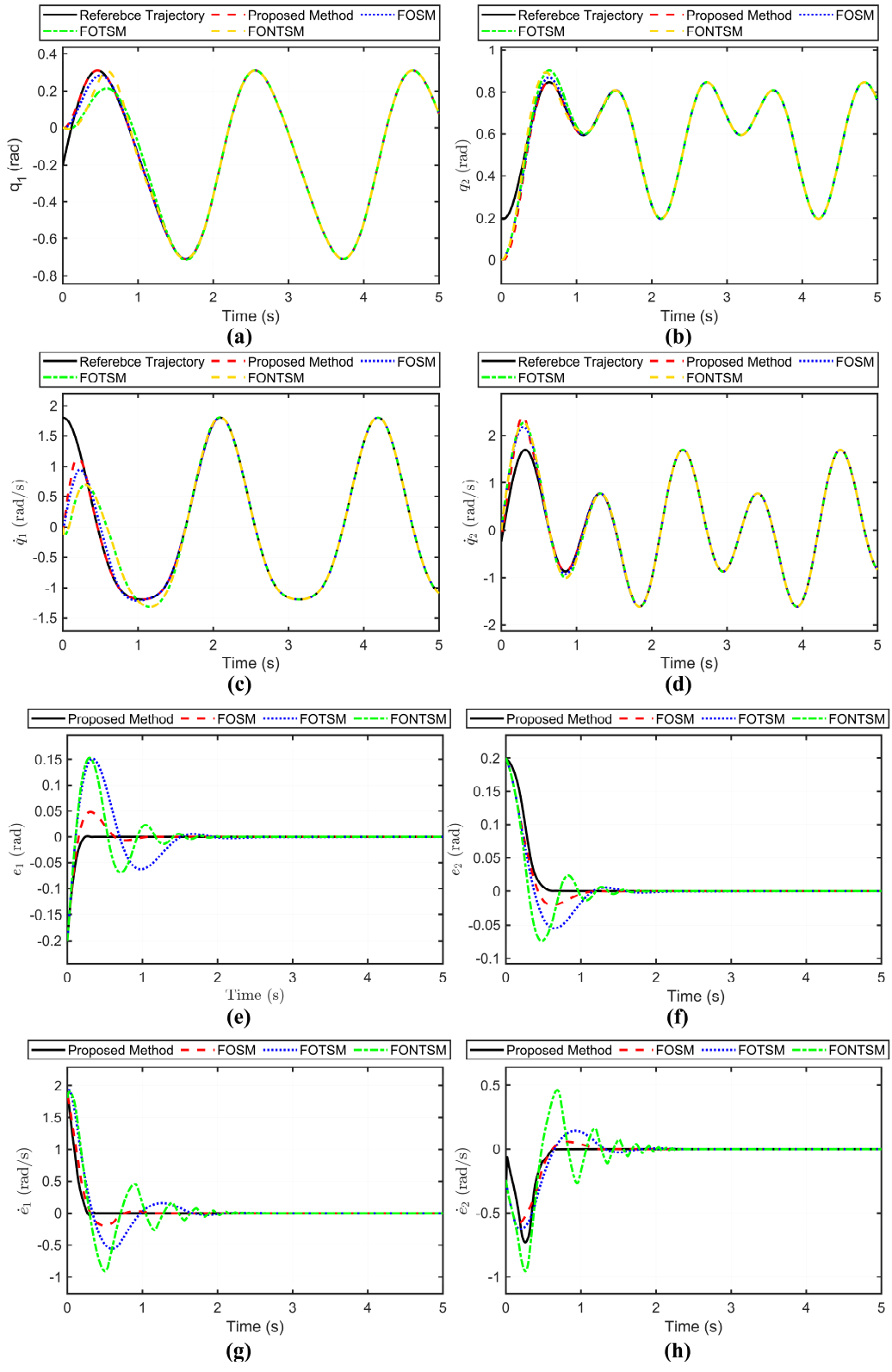


Figure 7. Tracking performance of joint positions and angular velocities. (**a**) Position trajectory of Joint 1. (**b**) Position trajectory of Joint 2. (**c**) Angular velocity trajectory of Joint 1. (**d**) Angular velocity trajectory of Joint 2. (**e**) Position tracking error of Joint 1. (**f**) Position tracking error of Joint 2. (**g**) Angular velocity tracking error of Joint 1. (**h**) Angular velocity tracking error of Joint 2.

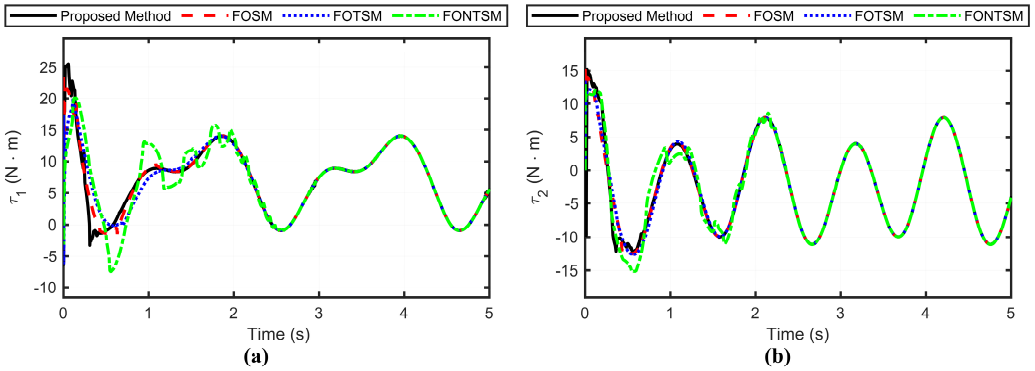


Figure 8. Control torques of the joints. (**a**) Joint 1. (**b**) Joint 2.

The quantitative comparison results are summarized in Table 4. The proposed Fuzzy PID-FOTSMC achieves position-tracking convergence times of 0.223 s and 0.556 s for Joints 1 and 2, respectively, outperforming all three benchmark controllers. Furthermore, the proposed method yields the lowest steady-state position tracking errors for both joints, demonstrating improved tracking accuracy under model uncertainties and external disturbances. Although the proposed method requires a relatively higher peak control torque for Joint 1, its superior convergence performance and steady-state accuracy demonstrate the effectiveness of the integrated observer–controller framework.

Although the proposed method requires a relatively higher peak control torque for Joint 1, the results demonstrate that the proposed observer–controller framework achieves faster convergence and improved steady-state tracking accuracy. These findings highlight the effectiveness of the proposed control strategy in balancing tracking performance and control effort.

Overall, the simulation results demonstrate that the proposed Fuzzy PID-FOTSMC achieves faster convergence and higher steady-state tracking accuracy than the benchmark controllers under model uncertainties and external disturbances. The quantitative results further confirm the effectiveness of the integrated observer–controller framework in improving trajectory-tracking performance while maintaining bounded control inputs.

5.4. Ablation Study

To evaluate the contributions of the proposed control components, three ablation configurations were considered under the same simulation conditions as in Section 5.3: Without Fuzzy PID (fixed PID gains), Without FO (fractional-order terms removed), and Without IFODOB (disturbance observer compensation disabled). Figure 9 presents the position and angular-velocity tracking errors of both joints, while Table 5 summarizes the steady-state mean absolute errors (SS-MAE) over 3–5 s.

As shown in Figure 9 and Table 5, the fuzzy PID gains play different roles in tracking performance: the proportional gain mainly accelerates error correction, the integral gain helps reduce steady-state errors, and the derivative gain provides damping to suppress overshoot and oscillations. Removing fuzzy gain adaptation increases the steady-state angular-velocity MAE of Joint 1 from 0.000968 to 5.657881 ($\times 10^{-3}$ rad/s), highlighting the benefit of adaptive PID tuning. Furthermore, the fractional-order parameters affect the sliding-surface dynamics and transient response, while the IFODOB parameters influence disturbance estimation and compensation performance. Disabling fractional-order terms or disturbance compensation leads to increased tracking errors, as demonstrated in Figure 9 and Table 5.

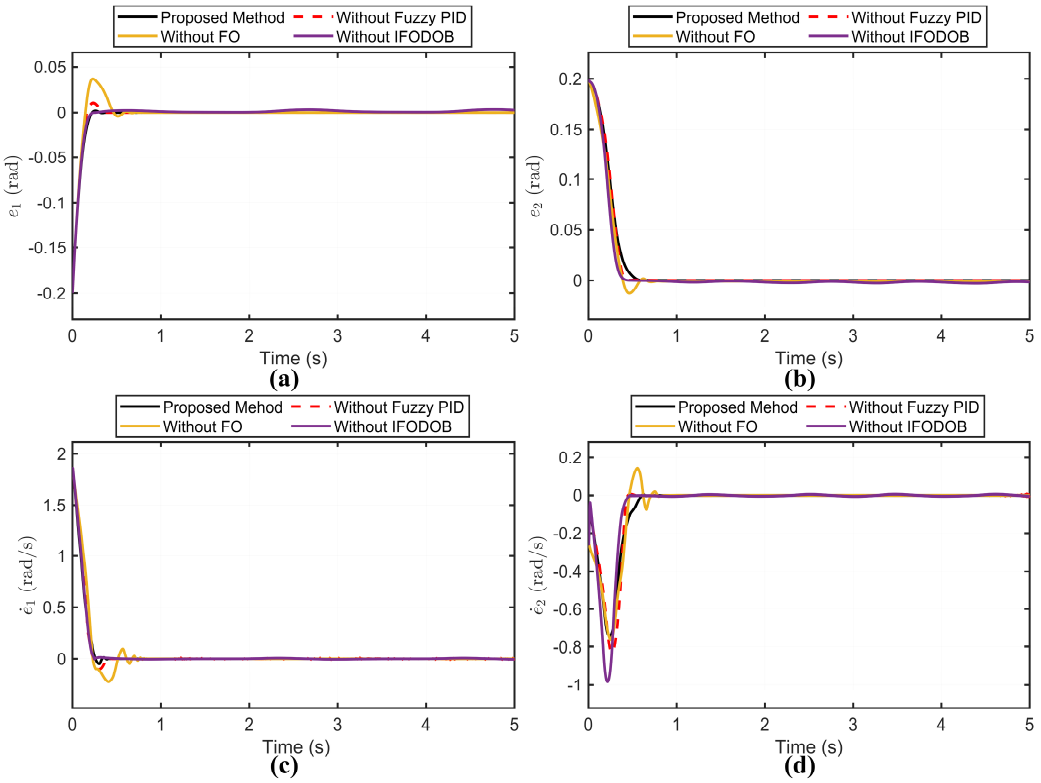


Figure 9. Tracking errors in the ablation study: (**a**) Joint 1 position error; (**b**) Joint 2 position error; (**c**) Joint 1 angular-velocity error; (**d**) Joint 2 angular-velocity error.

Table 5. Steady-state position and angular-velocity tracking errors in the ablation study.

Joint	Control Configuration	Position SS-MAE ($\times 10^{-3}$ rad)	Velocity SS-MAE ($\times 10^{-3}$ rad/s)
1	Proposed Method	0.000160	0.000968
1	Without Fuzzy PID	0.006514	5.657881
1	Without FO	0.007986	0.003358
1	Without IFODOB	1.486060	2.608766
2	Proposed Method	0.001785	0.001616
2	Without Fuzzy PID	0.004714	0.646929
2	Without FO	0.649085	0.079024
2	Without IFODOB	1.972793	3.088972

Overall, the ablation results demonstrate that fuzzy gain adaptation improves tracking accuracy, fractional-order dynamics enhance transient performance, and IFODOB compensation suppresses residual tracking errors under uncertainties and disturbances. Their combined effects contribute to the improved tracking performance of the proposed controller.

6. Conclusions

This paper proposes a Fuzzy PID-FOTSMC scheme integrated with an IFODOB for robotic manipulator trajectory tracking under uncertainties and external disturbances. Lyapunov-based analysis establishes practical finite-time convergence under the stated assumptions. Simulation results show that the IFODOB reduces the disturbance-estimation convergence times from 1.20 s and 1.30 s to 0.26 s and 0.27 s for Joints 1 and 2, respectively, while reducing the steady-state estimation error bound from ±0.15 N·m to ±0.03 N·m. The proposed controller also achieves position-tracking convergence times of 0.223 s and 0.556 s

for the two joints, outperforming three benchmark controllers in convergence speed and steady-state tracking accuracy.

Nevertheless, the proposed method has certain limitations. Its effectiveness has been verified only through numerical simulations on a planar two-DOF manipulator, while practical implementation may be affected by measurement noise, acceleration estimation errors, and computational complexity. To address these limitations, signal filtering and state observers could be employed to mitigate measurement noise and acceleration estimation errors, respectively. Computational complexity could be reduced through efficient numerical approximations of fractional-order operators and simplified fuzzy inference.

Future work will focus on experimental validation using physical robotic manipulators, with particular attention to measurement-noise robustness and accurate disturbance estimation. In addition, the real-time implementation of fractional-order operations and fuzzy gain adaptation will be investigated. The proposed framework will also be extended to more complex multi-DOF manipulators to evaluate its applicability under realistic operating conditions.

Author Contributions: Conceptualization, J.L. and S.S.; methodology, J.L.; software, J.L.; validation, M.J. and H.L.; formal analysis, J.L. and Z.L.; investigation, M.J.; resources, S.S.; data curation, H.L.; writing—original draft preparation, J.L.; writing—review and editing, S.S.; visualization, J.L.; supervision, Z.L.; project administration, S.S.; funding acquisition, H.L. All authors have read and agreed to the published version of the manuscript.

Funding: This work was supported by the Fundamental and Interdisciplinary Disciplines Breakthrough Plan of the Ministry of Education of China (JYB2025XDXM215) and the National Natural Science Foundation of China (Nos. T2388101 and 62403171).

Data Availability Statement: The data presented in this study are available on request from the corresponding author. The data are not publicly available due to privacy restrictions.

Conflicts of Interest: The authors declare no conflicts of interest. The funders had no role in the design of the study; in the collection, analyses, or interpretation of data; in the writing of the manuscript; or in the decision to publish the results.

References

1. Flores-Abad, A.; Ma, O.; Pham, K.; Ulrich, S. A Review of Space Robotics Technologies for On-Orbit Servicing. *Prog. Aerosp. Sci.* **2014**, *68*, 1–26. [CrossRef]
2. Ruggiero, D.; Basnayake, I.; Park, H.; Capello, E. Attitude and Position Control for Formation Flying of Space Robots Equipped with a Robotic Manipulator. *Acta Astronaut.* **2024**, *222*, 596–608. [CrossRef]
3. Fallahiarezoodar, N.; Zhu, Z.H. Review of Autonomous Space Robotic Manipulators for On-Orbit Servicing and Active Debris Removal. *Space Sci. Technol.* **2025**, *5*, 0291. [CrossRef]
4. Mirza, J.; Kanwal, F.; Salaria, U.A.; Ghafoor, S.; Aziz, I.; Atieh, A.; Almogren, A.; Haq, A.U.; Kanwal, B. Underwater Temperature and Pressure Monitoring for Deep-Sea SCUBA Divers Using Optical Techniques. *Front. Phys.* **2024**, *12*, 1417293. [CrossRef]
5. Zhan, B.; Jin, M.; Yang, G.; Huang, B. Finite-Time Adaptive Control for the Dual-Arm Space Robots with Uncertain Kinematics, Dynamics and Dead-Zone Nonlinearities. *Proc. Inst. Mech. Eng. C J. Mech. Eng. Sci.* **2021**, *235*, 6435–6450. [CrossRef]
6. Zhang, L.; Liu, H.; Tang, D.; Hou, Y.; Wang, Y. Adaptive Fixed-Time Fault-Tolerant Tracking Control and Its Application for Robot Manipulators. *IEEE Trans. Ind. Electron.* **2022**, *69*, 2956–2966. [CrossRef]
7. Villecco, A.; Formato, A.; Cattani, P.; Villecco, F. Sizing the Actuators for a Dragon Fly Prototype. *J. Appl. Comput. Mech.* **2024**, *10*, 152–163. [CrossRef]
8. Armghan, A.; Alsharari, M.; Aliqab, K.; Alrashdi, I.; Kanwal, B.; Mirza, J.; Aziz, I. High-Speed and Potentially Scalable UWOC/UWB Converged Transmission Link for Underwater Wireless Optical Sensor Networks. *Front. Phys.* **2025**, *13*, 1650284. [CrossRef]
9. Zhu, N.; Gao, X.-T.; Huang, C.-Q. A Data-Driven Approach for on-Line Auto-Tuning of Minimum Variance PID Controller. *ISA Trans.* **2022**, *130*, 325–342. [CrossRef] [PubMed]
10. Rybus, T.; Seweryn, K.; Sasiadek, J.Z. Control System for Free-Floating Space Manipulator Based on Nonlinear Model Predictive Control (NMPC). *J. Intell. Robot. Syst.* **2017**, *85*, 491–509. [CrossRef]

11. Ghasemi, M.; Nersesov, S.G.; Clayton, G. Finite-Time Tracking Using Sliding Mode Control. *J. Frankl. Inst.* **2014**, *351*, 2966–2990. [CrossRef]
12. Barkana, I. Robustness and Perfect Tracking in Simple Adaptive Control. *Int. J. Adapt. Control Signal Process.* **2016**, *30*, 1118–1151. [CrossRef]
13. Hassan, M.; Aljuwaiser, E.; Badr, R. A New On-Line Observer-Based Controller for Leader-Follower Formation of Multiple Nonholonomic Mobile Robots. *J. Frankl. Inst.* **2018**, *355*, 2436–2472. [CrossRef]
14. Slotine, J.J.; Sastry, S.S. Tracking Control of Non-Linear Systems Using Sliding Surfaces, with Application to Robot Manipulators†. *Int. J. Control* **1983**, *38*, 465–492. [CrossRef]
15. Xu, S.S.-D.; Chen, C.-C.; Wu, Z.-L. Study of Nonsingular Fast Terminal Sliding-Mode Fault-Tolerant Control. *IEEE Trans. Ind. Electron.* **2015**, *62*, 3906–3913. [CrossRef]
16. Wang, H.; Ye, X.; Tian, Y.; Zheng, G.; Christov, N. Model-Free–Based Terminal SMC of Quadrotor Attitude and Position. *IEEE Trans. Aerosp. Electron. Syst.* **2016**, *52*, 2519–2528. [CrossRef]
17. Feng, Y.; Yu, X.; Man, Z. Non-Singular Terminal Sliding Mode Control of Rigid Manipulators. *Automatica* **2002**, *38*, 2159–2167. [CrossRef]
18. Yu, X.; Zhihong, M. Fast Terminal Sliding-Mode Control Design for Nonlinear Dynamical Systems. *IEEE Trans. Circuits Syst. I* **2002**, *49*, 261–264. [CrossRef]
19. Wang, J.; Zhao, Z.; Zheng, Y. NFTSM-Based Fault Tolerant Control for Quadrotor Unmanned Aerial Vehicle with Finite-Time Convergence. *IFAC-PapersOnLine* **2018**, *51*, 441–446. [CrossRef]
20. Li, Y.; Xu, Q. Adaptive Sliding Mode Control With Perturbation Estimation and PID Sliding Surface for Motion Tracking of a Piezo-Driven Micromanipulator. *IEEE Trans. Control Syst. Technol.* **2010**, *18*, 798–810. [CrossRef]
21. Qi, M.; Han, S.; Guo, G.; Liu, P.; Zhi, Y.; Zhao, Z. Adaptive Trajectory Tracking Control of Robotic Manipulators Based on Integral Sliding Mode. *Asian J. Control* **2025**, *27*, 1361–1372. [CrossRef]
22. Dinh, X.-M.; Luong, T.-G.; Le, X.-H.; Nguyen, V.-T.; Kim, D.-T. Adaptive Fuzzy Dynamic Surface Control with Sliding Mode Control for Enhanced Trajectory Tracking of Delta Robots. *J. Control Autom. Electr. Syst.* **2025**, *36*, 611–635. [CrossRef]
23. Baik, I.C.; Kim, K.H.; Youn, M.J. Robust Nonlinear Speed Control of PM Synchronous Motor Using Boundary Layer Integral Sliding Mode Control Technique. *IEEE Trans. Control Syst. Technol.* **2000**, *8*, 47–54. [CrossRef]
24. Fallaha, C.J.; Saad, M.; Kanaan, H.Y.; Al-Haddad, K. Sliding-Mode Robot Control With Exponential Reaching Law. *IEEE Trans. Ind. Electron.* **2011**, *58*, 600–610. [CrossRef]
25. Utkin, V.; Poznyak, A.; Orlov, Y.; Polyakov, A. Conventional and High Order Sliding Mode Control. *J. Frankl. Inst.* **2020**, *357*, 10244–10261. [CrossRef]
26. Liu, Z.; Liu, J.; Zhang, O.; Zhao, Y.; Chen, W.; Gao, Y. Adaptive Disturbance Observer-Based Fixed-Time Tracking Control for Uncertain Robotic Systems. *IEEE Trans. Ind. Electron.* **2024**, *71*, 14823–14831. [CrossRef]
27. Jing, C.; Zhang, H.; Yan, B.; Hui, Y.; Xu, H. State and Disturbance Observer Based Robust Disturbance Rejection Control for Friction Electro-Hydraulic Load Simulator. *Nonlinear Dyn.* **2024**, *112*, 17241–17255. [CrossRef]
28. Zhu, Y.; Qiao, J.; Guo, L. Adaptive Sliding Mode Disturbance Observer-Based Composite Control With Prescribed Performance of Space Manipulators for Target Capturing. *IEEE Trans. Ind. Electron.* **2019**, *66*, 1973–1983. [CrossRef]
29. Qiao, J.; Wu, H.; Yu, X. High-Precision Attitude Tracking Control of Space Manipulator System Under Multiple Disturbances. *IEEE Trans. Syst. Man Cybern. Syst.* **2021**, *51*, 4274–4284. [CrossRef]
30. Kim, H.; Shim, H.; Jo, N.H.; Ataei, M.; Park, G. A Sliding Mode Approach to Asymptotic Recovery of Nominal Performance for Uncertain Linear Systems. *IEEE Trans. Ind. Electron.* **2026**, *73*, 2896–2904. [CrossRef]
31. Deng, Y.; Wang, J.; Li, H.; Liu, J.; Tian, D. Adaptive Sliding Mode Current Control with Sliding Mode Disturbance Observer for PMSM Drives. *ISA Trans.* **2019**, *88*, 113–126. [CrossRef] [PubMed]
32. Chen, K.-Y. Robust Optimal Adaptive Sliding Mode Control with the Disturbance Observer for a Manipulator Robot System. *Int. J. Control Autom. Syst.* **2018**, *16*, 1701–1715. [CrossRef]
33. Alyoussef, F.; Kaya, I. Improved Adaptive Dynamic Non-Singular Terminal Sliding Mode Controller with Fractional Disturbance Observer. *Inform. Sci.* **2023**, *641*, 119110. [CrossRef]
34. Wang, Y.; Yan, H.; Zhang, H.; Shen, H.; Lam, H.-K. Interval Type-2 Fuzzy Control for HMM-Based Multiagent Systems via Dynamic Event-Triggered Scheme. *IEEE Trans. Fuzzy Syst.* **2022**, *30*, 3063–3073. [CrossRef]
35. Zheng, Y.; Liu, Y.; Song, R.; Ma, X.; Li, Y. Adaptive Neural Control for Mobile Manipulator Systems Based on Adaptive State Observer. *Neurocomputing* **2022**, *489*, 504–520. [CrossRef]
36. Hu, Y.; Yan, H.; Zhang, H.; Wang, M.; Zeng, L. Robust Adaptive Fixed-Time Sliding-Mode Control for Uncertain Robotic Systems With Input Saturation. *IEEE Trans. Cybern.* **2023**, *53*, 2636–2646. [CrossRef] [PubMed]
37. Wang, H.-D.; Zhai, Y.-X.; Shah, U.H.; Karkoub, M.; Li, M. Adaptive Fuzzy Control of Underwater Vehicle Manipulator System with Dead-Zone Band Input Nonlinearities via Fuzzy Performance and Disturbance Observers. *Ocean Eng.* **2023**, *277*, 114194. [CrossRef]

38. Yang, X.; Zhao, Z.; Li, Y.; Yang, G.; Zhao, J.; Liu, H. Adaptive Neural Network Control of Manipulators with Uncertain Kinematics and Dynamics. *Eng. Appl. Artif. Intell.* **2024**, *133*, 107935. [CrossRef]
39. Wang, Y.; Gu, L.; Xu, Y.; Cao, X. Practical Tracking Control of Robot Manipulators With Continuous Fractional-Order Nonsingular Terminal Sliding Mode. *IEEE Trans. Ind. Electron.* **2016**, *63*, 6194–6204. [CrossRef]
40. Yaşkıran, B.; Öztürk, M.; Gökçe, B. Review of SMC and FOSMC Strategies for Rotary Wing UAVs. *Fractal Fract.* **2026**, *10*, 200. [CrossRef]
41. Muñoz-Vázquez, A.-J.; Parra-Vega, V.; Sánchez-Orta, A. Uniformly Continuous Differintegral Sliding Mode Control of Nonlinear Systems Subject to Holder Disturbances. *Automatica* **2016**, *66*, 179–184. [CrossRef]
42. Pouzesh, M.; Mobayen, S. Event-Triggered Fractional-Order Sliding Mode Control Technique for Stabilization of Disturbed Quadrotor Unmanned Aerial Vehicles. *Aerosp. Sci. Technol.* **2022**, *121*, 107337. [CrossRef]
43. Sun, G.; Ma, Z. Practical Tracking Control of Linear Motor With Adaptive Fractional Order Terminal Sliding Mode Control. *IEEE/ASME Trans. Mechatron.* **2017**, *22*, 2643–2653. [CrossRef]
44. Chaudhary, K.S.; Kumar, N. Fractional Order Fast Terminal Sliding Mode Control Scheme for Tracking Control of Robot Manipulators. *ISA Trans.* **2023**, *142*, 57–69. [CrossRef] [PubMed]
45. Yao, Y.; Ding, L.; Wang, Y. Fractional-Order Nonsingular Terminal Sliding Mode Control of a Cable-Driven Aerial Manipulator Based on RBF Neural Network. *Int. J. Aeronaut. Space Sci.* **2024**, *25*, 759–771. [CrossRef]
46. Yang, J.; Guo, T.; Yu, Y.; Jiang, P.; Cao, C.; Pang, X.; Dong, Q.; Wang, X. Adaptive Fuzzy Fractional-Order Terminal Sliding Mode Control Using Adaptive Neural Network Observation Architecture with Application to Ultra-Precision Stages. *Control Eng. Pract.* **2025**, *165*, 106623. [CrossRef]
47. Lin, X.; Wang, Y.; Liu, Y. Neural-Network-Based Robust Terminal Sliding-Mode Control of Quadrotor. *Asian J. Control* **2022**, *24*, 427–438. [CrossRef]
48. Al-Dujaili, A.Q.; Falah, A.; Humaidi, A.J.; Pereira, D.A.; Ibraheem, I.K. Optimal Super-Twisting Sliding Mode Control Design of Robot Manipulator: Design and Comparison Study. *Int. J. Adv. Robot. Syst.* **2020**, *17*, 1729881420981524. [CrossRef]
49. Nojavanzadeh, D.; Badamchizadeh, M. Adaptive Fractional-Order Non-Singular Fast Terminal Sliding Mode Control for Robot Manipulators. *IET Control Theory Appl.* **2016**, *10*, 1565–1572. [CrossRef]
50. Kilbas, A.A.; Srivastava, H.M.; Trujillo, J.J. *Theory and Applications of Fractional Differential Equations*, 1st ed.; Elsevier Science: Amsterdam, The Netherlands, 2006; Volume 204.
51. Muñoz-Vázquez, A.J.; Sánchez-Torres, J.D.; Parra-Vega, V.; Sánchez-Orta, A.; Martínez-Reyes, F. A Fractional Super-Twisting Control of Electrically Driven Mechanical Systems. *Trans. Inst. Meas. Control* **2020**, *42*, 485–492. [CrossRef]
52. Dou, B.; Yue, X. Disturbance Observer-Based Fractional-Order Sliding Mode Control for Free-Floating Space Manipulator with Disturbance. *Aerosp. Sci. Technol.* **2023**, *132*, 108061. [CrossRef]
53. Shao, X.; Sun, G.; Yao, W.; Li, X.; Zhang, O. Fractional-Order Resolved Acceleration Control for Free-Floating Space Manipulator with System Uncertainty. *Aerosp. Sci. Technol.* **2021**, *118*, 107041. [CrossRef]

Disclaimer/Publisher's Note: The statements, opinions and data contained in all publications are solely those of the individual author(s) and contributor(s) and not of MDPI and/or the editor(s). MDPI and/or the editor(s) disclaim responsibility for any injury to people or property resulting from any ideas, methods, instructions or products referred to in the content.